A PROGRAMMING MODEL FOR ANALYZING THE MECHANICAL AND THERMAL BUCKLING BEHAVIOR OF ECO-CONCRETE PANELS INCORPORATING RECYCLED WASTE MATERIALS (GLASS AND RED BRICKS)

UM MODELO DE PROGRAMAÇÃO PARA ANALISAR O COMPORTAMENTO DE FLAMBAGEM MECÂNICA E TÉRMICA DE PAINÉIS DE CONCRETO ECOLÓGICO INCORPORANDO MATERIAIS RESIDUAIS RECICLADOS (VIDRO E TIJOLOS VERMELHOS)

> Article received on: 05/05/2025 Article accepted on: 08/19/2025

Abdelkader Yerkrou*

* Laboratory of Advanced Structures and Materials in Civil Engineering and Public Works, Sidi Bel Abbes, Algeria Orcid: https://orcid.org/0009-0002-6194-9976 abdelkader.yekrou@univ-sba.dz

Abdelmoutalib Benfrid *

* Laboratory of Advanced Structures and Materials in Civil Engineering and Public Works, Sidi Bel Abbes, Algeria Orcid: https://orcid.org/0009-0007-8171-1654 benfridabdelmoutalib2050@gmail.com

Baghdad Krour*

* Laboratory of Advanced Structures and Materials in Civil Engineering and Public Works, Sidi Bel Abbes, Algeria Orcid: https://orcid.org/0000-0002-8265-9807 krour.bag@gmail.com

Mohamed Bachir Bouiadjra *

* Laboratory of Advanced Structures and Materials in Civil Engineering and Public Works, Sidi Bel Abbes, Algeria Orcid: https://orcid.org/0009-0008-4814-6187

mohamedbachirbouiadjra@gmail.com

The authors declare that there is no conflict of interest



Abstract

In today's world, there is an accumulation of glass waste and red brick waste due to several factors. These materials have a significant impact on environmental protection. Among the proposed solutions, incorporating a certain percentage of these wastes into concrete offers an interesting alternative. In this paper, the study focuses on the mechanical and thermal buckling behavior of concrete incorporating declared waste for panel applications. The study aims to develop a program to obtain the thermo-mechanical properties of a biphasic concrete mixture incorporating waste. The adopted model is the Mori-Tanaka model. The same program will then be used to determine the critical buckling load and the variation in the critical buckling temperature based on the first-order shear deformation theory (FSDT) with a correction factor of 5/6. It is clearly demonstrated that the inclusion of waste improves mechanical properties, but negatively affects thermal properties. Similarly, the critical buckling efforts are influenced by this waste incorporation. It is observed that brick waste yields better results compared to glass waste in terms of thermal buckling.

Keywords: Glass Waste. Red Brick Waste. Eco-concrete. Thermo-mechanical Properties. Mori-Tanaka Model. Buckling Behavior.

Resumo

No mundo atual, há um acúmulo de resíduos de vidro e tijolos vermelhos devido a diversos fatores. Esses materiais têm um impacto significativo na proteção ambiental. Entre as soluções propostas, a incorporação de uma determinada porcentagem desses resíduos ao concreto oferece uma alternativa interessante. Neste artigo, o estudo se concentra no comportamento de flambagem mecânica e térmica do concreto com incorporação de resíduos declarados para aplicações em painéis. O objetivo do estudo é desenvolver um programa para obter as propriedades termomecânicas de uma mistura de concreto bifásica com incorporação de resíduos. O modelo adotado é o modelo de Mori-Tanaka. O mesmo programa será então utilizado para determinar a carga crítica de flambagem e a variação da temperatura crítica de flambagem com base na teoria de deformação por cisalhamento de primeira ordem (FSDT) com um fator de correção de 5/6. É claramente demonstrado que a inclusão de resíduos melhora as propriedades mecânicas, mas afeta negativamente as propriedades térmicas. Da mesma forma, os esforços críticos de flambagem são influenciados por essa incorporação de resíduos. Observa-se que os resíduos de tijolo apresentam melhores resultados em comparação aos resíduos de vidro em termos de flambagem térmica.

Palavras-chave: Resíduos de Vidro. Resíduos de Tijolo Vermelho. Ecoconcreto. Propriedades Termomecânicas. Modelo Mori-Tanaka. Comportamento de Flambagem.

1 INTRODUCTION

The rate of glass waste and red brick waste is increasing in the environment every day. N. Guermoud et al. state that glass accounts for 2.8% of the total waste in Algeria, based on a statistical study conducted at the beach of Mostaghanem [1]. Sonia Akrour et al. link demographic growth to the increase in glass waste and highlight the environmental hazards posed by these wastes. They call for urgent intervention to address this issue and for the establishment of permanent legislation to prevent the accumulation of glass in Algeria, through effective management and direct recycling of glass waste [2]. Seyed Ali Delbari and Lucas A. Hof state that the accumulation of glass is approximately 21 million tons, with a very small proportion being recycled annually, which is a very low percentage compared to the glass production [3]. Chong Fu et al. show that in 2024, the glass recycling rate is below 34%, indicating a low feasibility for glass waste management, as these wastes no longer change their parameters in the management process [4]. Baojia Qin et al. report that in the USA, the glass recycling rate is 33% per year, while in China

it reaches 20% per year, but these two percentages remain low compared to the disposal of glass in public bins [5]. Mohammed Rihan Maaze and Sandeep Shrivastava demonstrate in a scientific paper that the investigation of these wastes in construction materials directly reduces CO₂ pollution [6]. Saloua El Euch Khay states that in Tunisia, by 2016, 5% of the 15 million tons of production were damaged [7]. Ingrid Silva Assis Santana et al. demonstrate through experience that brick waste can be reused as pozzolanic materials to increase the compressive strength of concrete [8]. Muhammad Saad Amjad and Nancy Diaz-Elsayed propose a perfect formulation using plastic waste to manufacture bricks, with a significant reduction in toxicity [9]. Ekaterina Kravchenko et al. demonstrate in 2025 that replacing high-performance brick powder with Portland cement reduces CO2 emissions in concrete [10].

It has been shown that these two types of waste cause negative effects on the environment. It is preferable to present some research findings that show that brick and glass waste can be used in concrete.

Daban A. Muhedin and Rahel K. Ibrahim produce concrete using ultra-fine glass powder. The results are excellent both in the short and long term, indicating that glass powder significantly enhances the mechanical properties of concrete [11]. Bimantara Putra Nugraha et al. state that recycled glass can be used as an additive in concrete, resulting in a 15% improvement in compressive strength [12]. Kaffayatullah Khan et al. demonstrate through experiments that glass powder extracted from waste improves the mechanical properties and durability of mortars, with a replacement of 5% to 25% of cement [13]. Zeybek et al. discuss the possibility of adding glass powder to concrete at a rate of 20% of the total cement content [14]. The experiments of Yan Diao et al. demonstrate the possibility of incorporating up to 30% glass micro-particles to achieve a strong and durable concrete [15]. Mohammed M. Salman et Mohammad Z. Yousif montrent qu'un remplacement de 10 % du ciment par de la poudre de verre peut améliorer de 13 % la résistance à la compression du béton [16]. Hajer Satih Abbas et al. practically demonstrate that brick waste results in lightweight concrete with improved compressive performance, showing a 7% increase compared to ordinary concrete [17]. Saif Saad Mansoor et al. find that brick waste reduces the weight of concrete by half and also improves the compressive strength by 14% [18]. Mohammed Salah Nasr et al. conduct experiments and show that concrete aggregates can be replaced by aggregates from brick waste, with an 11.98% increase in strength [19]. Mohammed Salah Nasr et al. conduct an

experiment where replacing 25% of the cement results in a 10% increase in strength compared to conventional concrete [20].

Several studies are conducted within the framework of analytical and programming approaches to study the different behaviors of structures, as well as for asymptotic homogenization in a periodic medium.

Benfrid et al. studied the thermoelastic bending behavior of a panel in concreteincorporating glass nanoparticles. They found that the glass nanoparticles negatively influence the thermal loading [21]. Harrat et al. study the bending behavior of a beam resting on an elastic foundation. They considered the effect of nano-silica agglomeration along the beam and adopted their homogenization using an advanced evaluation model [22]. Mohammed Chatbi studies the bending behavior of a plate resting on an elastic foundation. They considered the effect of nanosilica agglomeration at the edges and the center of the plate, along its length and width, and adopted their homogenization using a Voigt model [23]. Dine Elhennani et al. study the different mechanical behaviors of a beam reinforced with various types of nanoparticles within a concrete matrix [24]. Işık, E., et al. study the seismic vibration behavior on a reinforced concrete structure, considering the rupture mechanisms and vulnerabilities of buildings, and examining the various construction standards [25]. Işık, E., et al. specifically study the Kahramanmaraş earthquake to interpret the faults in structures caused by the propagation of this earthquake, and also assess the durability of these construction materials [26]. Harrat et al. study the thermoelastic behavior of a concrete slab reinforced with iron oxide nanoparticles. Homogenization was established using the Eshelby model [27]. Kecir et al. study a concrete slab reinforced with nano-sized iron oxide particles and investigate the slab's deflection. The stiffness matrix of the stress tensor is determined using the Eshelby model[28]. Chatbi et al. rely on the Eshelby model to deduce the mechanical properties of a slab reinforced with nano-clay particles [29]. Işık, E., et al. study the seismicity of Adıyaman and propose support solutions for buildings, given the seismic propagation and the failures they observed [30].

For homogenization, as we have seen, there are several models such as the Eshelby model used in the references already cited, as well as others; Mohammed Chatbi et al. study the vibration of a beam reinforced with carbon nanotubes randomly distributed. Local homogenization was established using the MORI-TANAKA model, and the carbon nanotubes enhance resistance to vibrations [31]. Benfrid et al. used the

LIWES model and NIELSON's SPAR model to homogenize concrete with organic nanofibers to study the energetic behavior of bio-concrete [32]. Benbakhti et al. employ the MORI-TANAKA model to improve the mechanical performance of a metal plate reinforced with tungsten nanoparticles [33]. Jing Zhou et al., in the context of predicting the elasticity of concrete, use various methods, among which the Mori-Tanaka model provided results that were very close [34]. Chanson Lu et al. study in depth the interfacial transition zone (ITZ) of fiber-reinforced concrete. This research is based on the Mori-Tanaka model for homogenization in a random medium [35]. Qing Chen et al. used the Mori-Tanaka model to predict the electromechanical properties of three inclusions in concrete in order to forecast the rehabilitation of this concrete and control its aging, as well as increase its service life [36]. Benfrid et al. used the HASEIN-STRIKMAN model to predict the elastic modulus, compressibility modulus, and shear modulus of concrete reinforced with glass nanoparticles [37]. Yao Wang et al. use the Mori-Tanaka model to determine the elastic modulus of a lightly reinforced ordinary concrete with fly ash inclusions. The results experimentally and theoretically demonstrate the approach [38]. Shirong Yan et al. adopt four micromechanical models, including the Voigt model, the Reuss model, the Eshelby method, and the Mori-Tanaka method, to predict the elastic modulus of recycled aggregate concrete [39]. The Mori-Tanaka model employs a homogenization approach grounded in the assumption that the average stress within the matrix is uniform across all positions. Additionally, the local fluctuating stress is incorporated into the average stress, with its mean value being zero over the entire matrix [40].

In structural analysis, there are several methods, among which; Krzysztof Murański et al. conduct a finite element analysis (FEA) of thin box-section columns under axial compression, with one end subjected to load and the other fixed. The study presents graphs related to the elastic central line, slope, deformation, as well as stress and strain states. Critical compression forces for 36 cases are determined based on slenderness ratios and cross-sectional shapes [41]. Albena Doicheva et al. study buckling and post-buckling using a numerical method under mechanical conditions to evaluate the actual load [42]. Albena Doicheva et al. provide an exact solution for the flexibility induced by buckling in the presence of the rigidity effect of a spring resting on a beam. This mathematical model is capable of solving this problem [43]. Mladenov, K. et al. conducted an instability analysis for a conical-shaped reservoir, where buckling induces a torsion effect [44].

Mladenov, K. et al. study the behavior of simply supported beams using the equipotential method to determine the maximum load for deflection and buckling [45]. Mladenov, K. et al. examine the buckling of beams combined with torsion effects, with deformations of various types, which introduces several parameters to be discussed in future research [46]. Doicheva, A. et al. contributed a mathematical model to determine the optimal critical load for deflection and buckling of beams at the support center [47]. Mladenov, K. et al. study the coupling between deflection and buckling using iterative mathematical methods [48]. Benfrid and Bachir Bouiadjra use a mathematical model to study the thermomechanical behavior of a panel in concretereinforced with glass nanoparticles at 10%, 20%, and 30%, based on the small deflection theory [49]. Kheitir et al. use continuous medium mechanics methods based on FSDT (First-Order Shear Deformation Theory) to determine the critical mechanical buckling load of a polymer plate reinforced with carbon nanotubes [50]. N. Enoma and J. Madu study the buckling behavior of circular-elliptical toroidal shells under external pressure using numerical methods, validated by extreme cases from the literature. The results show that these structures exhibit stable postbuckling behavior and can withstand loads higher than the elastic bifurcation point [51]. N. Enoma and J. Madu examine the impact of geometric imperfections on the buckling response of circular-elliptical toroidal shells under external pressure. Using the ABAQUS numerical method, they show that short tori are less sensitive to imperfections, while tall tori may experience up to a 70% reduction in buckling loads due to these imperfections [52]. Ike Charles Chinwuba derives the elastic stability equations for thick plates considering transverse deformation effects and solves the buckling problem using the Fourier series method. The results show that the thin plate theory significantly overestimates the critical buckling load of thick plates, providing safer and more accurate solutions [53]. I. Charles presents a formulation for the buckling of thick shear deformable plates using the variational method. The study provides an analytical solution for simply supported boundary conditions, considering transverse deformations and uniaxial and biaxial loads, confirming that the Fourier series method provides accurate solutions for the critical buckling loads [54]. Ike C. develops a buckling equation for shear deformable thick plates using a first-principles approach, solved by the Galerkin method for uniaxial and biaxial compressive loads. The equation is derived through total energy minimization and provides exact results for the critical buckling loads, confirmed by comparison with existing results. The novelty lies in the systematic method of formulating and solving the

Galerkin variational equation [55]. C. Ike and J. N. Ugwu use the Ritz method with a mathematical formulation to solve a mechanical buckling problem [56]. Peyyala Pramod Kumar et al. compare the buckling and deflection performances of CNT-reinforced composite beams using CLPT and FSDT theories, accounting for shear deformation effects and beam thickness. Their study employs the Mori-Tanaka approach to calculate the elastic constants based on the CNT reinforcement. [57]. Sushree Das and Prasun Jana conduct a buckling analysis of a rectangular isotropic plate subjected to a non-uniform load using the First-Order Shear Deformation Theory (FSDT). Their two-step method includes the evaluation of the stress distribution and stability analysis using the Galerkin method, with the critical buckling loads compared to published results for different aspect ratios of the plate [58]. Ivo Senjanović et al. present a first-order shear deformation plate theory based on Hamilton's principle, leading to a sixth-order partial differential equation. They compare the natural frequencies obtained with the Rayleigh-Ritz method in Mindlin's classical thick plate theory and assess the reliability of these theories [59]. P. J. Guruprasad and K. S. Pakhare present a new first-order shear deformation plate theory with a single variable, governed by a single fourth-order partial differential equation. This theory, based on a shear correction factor and yielding expressions similar to those of the classical plate theory, is demonstrated through comparative examples with other plate theories [60]. S.A.M. Ghannadpour et al. present an exact finite strip method for the buckling and post-buckling analysis of moderately thick plates using first-order shear deformation theory. They solve the Von-Karman equations to obtain out-of-plane modes and critical loads, assuming combined deformations after buckling [61]. B. Xu et al. investigate the buckling deformation of side plates in a concrete-filled steel tube (CFST) column under biaxial stress, using theoretical analysis, experimental validation, and finite element simulation. The results show that buckling behavior changes under biaxial stress, with an increase in the buckling coefficient and the number of buckling waves, as well as a relationship between the number of waves and the height-to-width ratio of the plate [62]. Stuart E. Swartz et al. develop four prediction equations based on orthotropic or isotropic behavior assumptions during buckling, applied to 24 reinforced concrete plates tested under uniaxial compression. The results show that the isotropic behavior assumption with the tangent modulus theory yields conservative but relatively accurate results [63]. Benfrid et al. use a physical model to predict the thermal buckling of plates reinforced by animal bones. They also rely on the FSDT theory [64]. X. Cheng presents

analytical solutions to study the thermal buckling of rectangular concrete plates simply supported or resting on elastic foundations [65]. Li-Cai Zhao et al. study the thermal buckling of damaged rectangular plates using continuum damage mechanics, considering the reduction in stiffness. The numerical results show that the inclusion of material damage improves the thermal buckling analysis and better meets design requirements in terms of reliability [66]. H. Wang et al. study the thermal buckling of annular sector plates made of concrete reinforced with nanocomposites using a mathematical modeling approach, solved by the Singular Discrete Convolution (DSC) method. Their approach combines deep neural network (DNN) predictions with DSC solutions to enhance the accuracy and efficiency of thermal buckling analysis [67]. Alexis Sauvageon et al. analyze the thermo-mechanical behavior of steel-concrete composite elements under high temperatures, with a focus on the thermal buckling of thin steel outer plates. Their integrated approach combines experimentation and numerical simulations to establish an analytical model used in the preliminary design of SC elements, validated by rigorous comparisons [68]. Minggui Zhou et al. study the post-thermal buckling behavior of eccentrically annular sector concrete plates reinforced with graphene oxide powders (GOP). Using the principle of minimum total potential energy and the Transformed Differential Quadrature Method (TDQM), they analyze the stability and thermal response of the plates, while integrating machine learning to predict complex phenomena and optimize the reinforced structures [69]. Alexis Sauvageon et al. conduct a parametric study of the buckling of SC elements under thermal loads, highlighting the impact of temperature uniformity and initial defects on the structural response. They propose a dimensional plastic buckling criterion and plan to study local deformations and extend the analysis to large-scale specimens [70].

This work is divided into three parts: the first aims to determine the mechanical and thermal properties of a biphasic concrete mix with additions of brick or glass powder, with homogenization carried out through programming scripts. The second part involves developing scripts to calculate the critical buckling force based on different concrete components with waste. Finally, the last step presents a script to determine the critical thermal variation for thermal buckling. This research paves the way for a better understanding of the thermal and mechanical behavior of panels reinforced with waste, thus contributing to the recycling of waste in concrete and the creation of eco-friendly materials.

2 HOMOGENIZATION MODEL

Several researchers use the Mori and Tanaka model [40] to predict the mechanical and thermal properties, in order to adopt the effective properties of new materials. The hypothesis of this work is to assume perfect cohesion between the matrix (concrete) and the reinforcement (brick or glass waste, in the form of ultra-fine powder) at the microscopic scale. It is assumed that the cohesion is perfect between the reinforcement and the grains, as well as the cement paste.

The abbreviations and symbols are defined as follows:

- E_c: The elasticity modulus of Concrete.
- Ew: The elasticity modulus of Waste.
- E_{hom}: The homogenized elasticity modulus.
- G_c: The shear modulus of Concrete.
- G_w: The shear modulus of Waste.
- G_{hom}: The homogenized shear modulus.
- K_c: The bulk modulus of Concrete.
- K_w: The bulk modulus of Waste.
- K_{hom}: The homogenized bulk modulus.
- v_c: The Poisson's ratio of Concrete.
- v_w: The Poisson's ratio of Waste.
- v_{hom}: The homogenized Poisson's ratio.
- V_c: The volume fractions of Concrete.
- V_w: The volume fractions of Waste.
- α_{hom} : The homogeneous thermal conductivity.
- α_c : The thermal expansion coefficient of Concrete.
- α_w : The thermal expansion coefficient of Waste.
- γ_{hom} : The homogeneous thermal conductivity.
- γ_c: The thermal conductivity of Concrete.

γ_w: The thermal conductivity of Waste

For the homogenization of the elastic modulus, the following steps are followed:

$$E_{hom} = \frac{9K_{hom}G_{hom}}{3K_{hom} + G_{hom}}; G_{hom} = G_c + \frac{V_wG_c(G_w - G_c)}{G_c + \beta_1(1 - V_w)(G_w - G_c)}; K_{hom} = K_c + \frac{V_wK_c(K_w - K_c)}{K_c + \beta_2(1 - V_w)(K_w - K_c)}$$
(1)

Where:

$$\beta_1 = \frac{2(4 - 5V_c)}{15(4 - 5V_c)}; \beta_2 = 3 - 5\beta_1$$
 (2)

It's noted that; $\beta 1$ and $\beta 2$ represent the correction coefficients for spherical inclusions (reinforcement by waste) in a metal matrix (concrete) [38-39-40].

$$K_c = \frac{E_c}{3(1 - 2\nu_c)}$$
 and $K_w = \frac{E_w}{3(1 - 2\nu_w)}$; $G_c = \frac{E_s}{2(1 + \nu_c)}$ and $G_w = \frac{E_w}{2(1 + \nu_w)}$

The properties of the individual isotropic materials (concrete and waste) are represented by the symbols $(K_c; K_w)$ and $(G_c; G_w)$ where the subscript «c" refers the concrete matrix and "w" refers the waste reinforcements. The homogenized Poisson's ratio is given by the following expression [40]:

$$\nu_{\text{hom}} = \frac{3K_{\text{hom}} - 2G_{\text{hom}}}{6K_{\text{hom}} + 2G_{\text{hom}}} \tag{4}$$

Based on the principle that the combined volume of the matrix and its reinforcement, as defined by the composite rule, equals one:

$$V_{Concrete+waste} = V_c + V_w = 1 \tag{5}$$

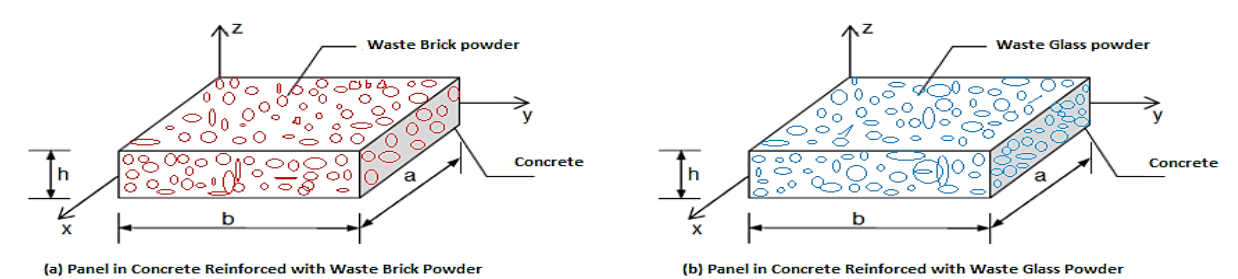
According to Mori and Tanaka [40], the expressions for thermal expansion and thermal conductivity can be given as follows:

$$\alpha_{\text{hom}} = \alpha_c - \frac{\lambda_w (\lambda_w (\lambda_w - (V_w \lambda_w + V_c \lambda_c))(\alpha_w - \alpha_c)}{(V_w \lambda_w + V_c \lambda_c)(\lambda_w - \lambda_c)}; \lambda_{\text{hom}} = \lambda_c + \frac{V_w \lambda_w (\lambda_w - \lambda_c)}{\lambda_c + \beta_1 (1 - V_w)(\lambda_w - \lambda_c)}$$
(6)

3 PROGRAMMING OF THE MECHANICAL AND THERMAL BUCKLING

In this section, the panel is simply supported, composed of concrete reinforced waste (brick and glass), as shown in Figure 1.

A simply supported concrete panel, reinforced with brick powder (a) and glass powder (b).



Gunjal Sachin M et al. use a refined displacement model to predict the critical buckling load [71]. B. M. Shinde et al. work with a trigonometric function of HSDT to calculate the deflection combined with buckling [72]. A. S. Sayyad uses various polygonal and trigonometric functions with HSDT displacement to obtain the stiffness matrix, then concludes the critical buckling load [73]. M. Bouazza and Adda create a mathematical model to derive a program capable of solving mechanical and thermal buckling [74]. Atteshamuddin S. Sayyad et al. predict a problem using the refined method to solve a bending and buckling problem [75]. Using these reference frameworks, we present our own calculation model that is capable of solving the critical buckling load and the critical temperature variation, and we apply the parameters of ordinary concrete and reinforced concrete to this programming.

The displacement components in the x, y, and z directions can be expressed as follows:

$$U(x,y,z) = u_0(x,y) - z \frac{\partial w_b(x,y)}{\partial x} - f(z) \frac{\partial w_s(x,y)}{\partial x}$$

$$\partial w_s(x,y) \qquad \partial w_s(x,y) \qquad \partial w_s(x,y)$$
(7)

$$V(x, y, z) = v_0(x, y) - z \frac{\partial w_b(x, y)}{\partial y} - f(z) \frac{\partial w_s(x, y)}{\partial y}$$
(8)

$$W(x, y, z) = w_b(x, y) + w_s(x, y)$$
 (9)

The displacements in the x and y directions at a point on the mid-plane of the panel are denoted as (u_0, v_0) , while (w_b, w_s) represent the buckling and shear components, respectively, of the transverse displacement f(z). The first order sear deformation theory is used

$$f(z) = z; g(z) = \frac{\partial f(z)}{\partial z}; \kappa_s = \frac{5}{6}$$
 (10)

The constitutive stress-strain relationships for the panel are defined as follows:

$$\begin{bmatrix} \sigma_{x} \\ \sigma_{y} \\ \tau_{xy} \\ \tau_{yz} \end{bmatrix} = \begin{bmatrix} \widehat{Q}_{11} & \widehat{Q}_{12} & 0 & 0 & 0 \\ \widehat{Q}_{21} & \widehat{Q}_{22} & 0 & 0 & 0 \\ 0 & 0 & \widehat{Q}_{33} & 0 & 0 \\ 0 & 0 & 0 & \widehat{Q}_{44} & 0 \\ 0 & 0 & 0 & 0 & \widehat{Q}_{55} \end{bmatrix} \begin{bmatrix} \varepsilon_{x} - \alpha_{\text{hom}} T \\ \varepsilon_{y} - \alpha_{\text{hom}} T \\ 2\gamma_{xy} \\ 2\gamma_{xz} \\ 2\gamma_{yz} \end{bmatrix}$$
(11)

 Q_{ij} represents the reduced elastic constants of the homogenized system (which is isotropic), incorporating both the waste reinforcement and the concrete matrix, derived by applying the Mori-Tanaka model, where:

$$\widehat{Q}_{11} = \widehat{Q}_{22} = \frac{(1 - v_{hom})E_{hom}}{(1 + v_{hom})(1 - 2v_{hom})}; \widehat{Q}_{12} = \widehat{Q}_{21} = \frac{v_{hom}E_{hom}}{(1 + v_{hom})(1 - 2v_{hom})}$$
(12)

$$\hat{Q}_{33} = \hat{Q}_{44} = \hat{Q}_{55} = G_{hom} = \frac{E_{hom}}{2(1 + V_{hom})}$$
(13)

The components of the different deformations and distortions of the panel are derived using the following equations:

$$\varepsilon_{x} = \frac{\partial U}{\partial x} + \alpha_{\text{hom}} T; \varepsilon_{y} = \frac{\partial V}{\partial y} + \alpha_{\text{hom}} T; 2\gamma_{xy} = \frac{\partial U}{\partial x} + \frac{\partial V}{\partial y}; 2\gamma_{xz} = \frac{\partial U}{\partial z} + \frac{\partial W}{\partial x}; 2\gamma_{yz} = \frac{\partial V}{\partial z} + \frac{\partial W}{\partial y}$$
(14)

The principle of virtual work is applied to determine the mechanical bending response of the panel:

$$\int_{0}^{t} (\delta U + \delta V) dt = 0 \tag{15}$$

 δU is given by the following expression and represents the virtual variations of the internal strain energy within this panel:

$$\delta U = \int_{0}^{A} \int_{\frac{-h}{2}}^{\frac{h}{2}} (\sigma_{x} \delta \varepsilon_{x} + \sigma_{y} \delta \varepsilon_{y} + \tau_{xy} \delta \gamma_{xy} + \tau_{yz} \delta \gamma_{yz} + \tau_{xz} \delta \gamma_{xz}) dA dz$$
 (16)

Introducing equations (14) to (16) into the previous equation (17), they yield:

$$\delta U = \int_{A} \left(N_{x} \frac{\partial \delta u_{0}}{\partial x} - M^{b}_{x} \frac{\partial^{2} \delta w_{b}}{\partial^{2} x} + M^{s}_{x} \frac{\partial^{2} \delta w_{s}}{\partial^{2} x} + N_{y} \frac{\partial \delta v_{0}}{\partial y} - M^{b}_{x} \frac{\partial^{2} \delta w_{b}}{\partial^{2} y} + M^{s}_{x} \frac{\partial^{2} \delta w_{s}}{\partial^{2} y} + M^{s}_{x} \frac{\partial^{2} \delta w_{s}}{\partial x \partial y} + 2M^{s}_{x} \frac{\partial^{2} \delta w_{s}}{\partial x \partial y} + Q_{yz} \frac{\partial \delta w_{s}}{\partial y} + Q_{xz} \frac{\partial \delta w_{s}}{\partial x}$$

$$(17)$$

The resultants of stresses and moments (N, M_b , M_s , Q (mechanical case) and N^T , M^{T}_{b} , M^{T}_{s} , Q^{T} (thermal case)):

$$N_{ij} = b \int_{\frac{-h}{2}}^{\frac{-h}{2}} \sigma_{ij} dz ; M^{b}_{ij} = b \int_{\frac{-h}{2}}^{\frac{-h}{2}} z \sigma_{ij} dz ; M^{s}_{ij} = b \int_{\frac{-h}{2}}^{\frac{-h}{2}} f(z) \sigma_{ij} dz ; Q_{ij} = b \int_{\frac{-h}{2}}^{\frac{-h}{2}} g(z) \kappa_{s} \sigma_{ij} dz$$

$$N^{T}_{ij} = b \int_{\frac{-h}{2}}^{\frac{-h}{2}} \sigma_{ij} dz ; M^{bT}_{ij} = b \int_{\frac{-h}{2}}^{\frac{-h}{2}} z \sigma_{ij} dz ; M^{sT}_{ij} = b \int_{\frac{-h}{2}}^{\frac{-h}{2}} f(z) \sigma_{ij} dz ; Q^{T}_{ij} = b \int_{\frac{-h}{2}}^{\frac{-h}{2}} g(z) \kappa_{s} \sigma_{ij} dz$$

$$(18)$$

Note that i or j correspond to x or y.

 δV represents the virtual external energy induced by the external mechanical buckling loads (N (mechanical loads) and T (Thermal Loads)) and is defined as:

$$\delta V = -\int_{A} \int_{\frac{-h}{2}}^{\frac{h}{2}} N \delta W dA dz; \delta V = -\int_{A} \int_{\frac{-h}{2}}^{\frac{h}{2}} T \delta W dA dz$$
 (19)

By substituting equation (19 and 18) with equation (17), which depends on equation (20), and performing integration by parts while considering the coefficients of δu_0 , δv_0 , δw_b and δw_s , the resulting equations of motion are derived as follows:

$$\delta u_0 : \frac{\partial N_x}{\partial x} + \frac{\partial N_{xy}}{\partial y} = 0 \tag{20}$$

$$\delta v_0 : \frac{\partial N_y}{\partial v} + \frac{\partial N_{xy}}{\partial x} = 0 \tag{21}$$

$$\delta w_b : \frac{\partial^2 M^b_{x}}{\partial x^2} - 2 \frac{\partial^2 M^b_{xy}}{\partial x \partial y} + \frac{\partial^2 M^b_{y}}{\partial y^2} + (N \text{ or } T) = 0$$
 (22)

$$\delta w_{s}: \frac{\partial^{2} M_{x}^{s}}{\partial x^{2}} - 2 \frac{\partial^{2} M_{xy}^{s}}{\partial x \partial y} + \frac{\partial^{2} M_{y}^{s}}{\partial y^{2}} + \frac{\partial Q_{xz}}{\partial x} + \frac{\partial Q_{yz}}{\partial y} + (N \text{ or } T) = 0$$
(23)

Given the simply supported rectangular panel, shown in Figure 1, with a length "a", a width "b", and a total thickness "h", the boundary conditions are defined as follows:

$$x = 0; x = a; v_0 = w_b = w_s = N_x = M_x^b = M_x^s = 0$$

$$y = 0; x = b; u_0 = w_b = w_s = N_y = M_y^b = M_y^s = 0$$
(24)

The Buckling loads

$$N = Nx + \lambda Ny; T = Tx \text{ or } Ty$$
 (25)

Using Navier's solution for the simply supported plate case, the admissible displacement functions will be expressed in the following manner to satisfy the boundary conditions outlined in the equation (35).

$$u(x,y) = \sum_{m=1}^{\infty} \sum_{n=1}^{\infty} X_{mn} \cos(\xi x) \sin(\zeta x)$$
 (26)

$$v(x,y) = \sum_{m=1}^{\infty} \sum_{n=1}^{\infty} Y_{mn} \cos(\xi x) \sin(\zeta x)$$
 (27)

$$w_b(x,y) = \sum_{m=1}^{\infty} \sum_{n=1}^{\infty} Z_{bmn} \sin(\xi x) \sin(\zeta x)$$
 (28)

$$w_s(x,y) = \sum_{m=1}^{\infty} \sum_{n=1}^{\infty} Z_{smn} \sin(\xi x) \sin(\zeta x)$$
 (29)

 $(X_{mn}, Y_{mn}, Z_{bmn}, Z_{smn})$ are the arbitrary parameters to be determined. Where:

$$\xi = \frac{m\pi}{a}; \zeta = \frac{n\pi}{b} \tag{30}$$

Finally, to derive the analytical solutions, the results of the substitution can be presented in the following matrix form:

It is recommended to opt for a reduced system.

$$\begin{bmatrix} K_{33} - N_{33} & K_{34} \\ K_{34} & K_{44} \end{bmatrix} \begin{Bmatrix} w_{bmn} \\ w_{smn} \end{Bmatrix} = \begin{Bmatrix} 0 \\ 0 \end{Bmatrix}; N := solve \begin{Bmatrix} Det \begin{bmatrix} K_{33} - N_{33} & K_{34} \\ K_{34} & K_{44} \end{bmatrix} \end{Bmatrix}$$
(32)

After resolve N in mechanical Loads (Dimensionless parameter):

$$N_{cr} = \frac{12(1 - v_c^2)a^2N}{E_c h^3}$$
 (33)

Nota:

If $\lambda = 1$ two direction for buckling.

If $\lambda = 0$ one direction of buckling.

For thermal

$$T = \frac{\Delta T}{h} \left(\frac{h}{2} + z\right) + T_f; \Delta T := T_i - T_f; N = \int_{\frac{-h}{2}}^{\frac{h}{2}} E_{\text{hom}} \alpha_{\text{hom}} \left(\frac{z}{h} + \frac{1}{2}\right) T dz.$$
 (34)

For thermal case applicate the rule (34) in matrix (32) and resolve ΔT . We noted that:

$$K_{11} = -A_{11}\xi^{2} - A_{33}\zeta^{2}; K_{12} = -\xi\zeta(A_{33} + A_{12}); K_{13} = B_{11}\xi^{3} + (2B_{66} + B_{12})\xi\zeta^{2}; K_{14} = B_{11}^{s}\xi^{3} + (2B_{66} + B_{12})\xi\zeta^{2}; K_{22} = -A_{11}\xi^{2} + A_{33}\zeta^{2}; K_{23} = -B_{22}\zeta^{3} + (2B_{33} + B_{12})\zeta\xi^{2}; K_{24} = -B_{22}\zeta^{3} + (2B_{33} + B_{12})\zeta\xi^{2}; K_{25} = -B_{22}\zeta^{3} + (2B_{33} + B_{22})\zeta\xi^{2}; K_{25} = -B_{22}\zeta^{2}; K_{25} = -B_{22}\zeta^{2};$$

$$\begin{split} K_{24} &= -B^{s}_{22} \varsigma^{3} + (2B^{s}_{33} + B^{s}_{12}) \varsigma \xi^{2}; K_{33} = -D_{11} \xi^{4} + 2(D_{12} + 2D_{33})(\varsigma \xi)^{2} + D_{22} \varsigma^{2}; \\ K_{34} &= -D^{s}_{11} \xi^{4} + 2(D^{s}_{12} + 2D^{s}_{33})(\varsigma \xi)^{2} + D^{s}_{22} \varsigma^{2}; N_{33} = \varsigma^{2} + \lambda \xi^{2} \\ K_{44} &= -A^{s*}_{11} \xi^{4} - 2(A^{s*}_{12} + 2A^{s*}_{33})(\varsigma \xi)^{2} + A^{s*}_{22} \varsigma^{2} + A^{c*}_{55} \xi^{2} + A^{c*}_{44} \varsigma^{2}; \\ (35) \end{split}$$

It's noted that:

$$A_{ij} = b \int_{-\frac{h}{2}}^{\frac{h}{2}} \widehat{Q}_{ij} dz; B_{ij} = b \int_{-\frac{h}{2}}^{\frac{h}{2}} \widehat{Q}_{ij} z dz; D_{ij} = b \int_{-\frac{h}{2}}^{\frac{h}{2}} \widehat{Q}_{ij} z^{2} dz; A^{s}_{ij} = b \int_{-\frac{h}{2}}^{\frac{h}{2}} \widehat{Q}_{ij} f(z) dz; B^{S}_{ij} = b \int_{-\frac{h}{2}}^{\frac{h}{2}} \widehat{Q}_{ij} z f(z) dz;$$
(36)

$$A^{s^*}_{ij} = b \int_{-\frac{h}{2}}^{\frac{h}{2}} \widehat{Q}_{ij} z \kappa_s f^2(z) dz; A^{c^*}_{ij} = b \int_{-\frac{h}{2}}^{\frac{h}{2}} \widehat{Q}_{ij} \kappa_s g(z) dz;$$
(37)

4 RESULTS AND DISCUSSION

The Mori and Tanaka model [40] is used in this study to obtain the various thermal and mechanical properties of concrete based on brick and glass waste, which will be used as reinforcements and cement replacements at an ultra-microfine scale in the form of powder. Table 1 shows the thermal and mechanical properties of the matrix (concrete) and the reinforcements (brick powder and glass powder). The effective properties after homogenization are illustrated in Table 2.

Table 1The initial mechanical properties of the matrix (concrete) and the two wastes (glass powder SiO_2 and brick powder Al_2O_3).

Properties	Matrix (Concrete)	Concrete	Reinforced (Waste)	Glass powder	Brick powder
		[21]		[21]	[76]
Elastic modulus	E_c (GPa)	20	E_c (GPa)	73	215
Poisson's ratio	ν_c	0.3	$ u_c$	0.16	0.22
Shear modulus	G _c (GPa)	7.79	G_c (GPa)	31.48	88.43
Bulk modulus	K_c (GPa)	16.67	K_c (GPa)	35.78	127.98
Thermal expansion	$a_c(10^{-6})(1/{}^{\circ}K)$	13.5	$\alpha_c(10^{-6})(1/{}^{\circ}K)$	0.55	8.9
Thermal conductivity	λ _c (W/m.°K)	1.75	λ _c (W/m.°K)	1.15	12

Properties	Elastic	Poisson's	Shear	Bulk	Thermal	Thermal
	modulus	ratio	modulus	modulus	expansion	conductivity
Symbols and	E _{hom}	$ u_{hom}$	G_{hom}	K _{hom}	$lpha_{hom}$	λ_{hom}
Units	(GPa)		(GPa)	(GPa)	(10 ⁻⁶)(1/°K)	(W/m.°K)
		Glas	ss Powder (SiC) ₂)		
Vw(0%)	20.00	0.30	7.69	16.67	13.50	1.75
Vw(10%)	25.30	0.27	9.94	18.52	12.62	1.70
Vw(20%)	30.56	0.25	12.22	20.38	11.67	1.65
Vw(30%)	33.18	0.23	14.53	22.26	10.65	1.60
	1	Bri	ck Powder (Al	₂ O ₃)	•	1
Vw(0%)	20.000	0.30	7.69	16.67	13.50	1.75
Vw(10%)	38.727	0.26	15.31	27.44	11.51	2.57
Vw(20%)	57.525	0.25	23.02	38.29	10.59	3.43
V _w (30%)	76.486	0.24	30.82	49.21	10.07	4.33

According to the results shown in Table 2, an improvement in mechanical properties is observed, such as the elastic modulus, which increases significantly with the addition of glass powder (+15 GPa at 30% glass powder) and even more substantially when using brick powder, with an almost threefold increase at 30%, which automatically leads to an improvement in compressibility modulus and shear modulus. Furthermore, the Poisson's ratio decreases slightly from 0.3 to 0.23 at 30%. Thermal expansion also decreases with every 10% addition of waste powder, though this decrease remains acceptable. Regarding conductivity, for the glass powder, the decrease is small but still shows a positive influence with the increase, while for brick powder, the improvement is more noticeable.

In Table 3, we compare our results with those from the literature and other researchers' works using the dimensionless parameter $\widehat{N} = \frac{Na^2}{h^3 E_c}$ and the elastic modulus of steel E=200GPa with a Poisson's ratio v=0.3 for a square plate a=b. This panel is isotropic. The comparison is made between the refined FSDT model and the results from Sayyad and Ghugal [75], as well as those from Charles Chinwuba Ike [54], the most recent work from 2025.

Table 3A comparison of the mechanical buckling \Re_{cr} of a square isotropic steel plate with variations in the thickness and width parameters for (uni/bi directional load).

The geometric ratio(a/h)	5	10	20	50	100	5	10	20	50	100
References		Unia	irection	al			Bid	irectiona	1	
Present (The refined FSDT)	2.9497	3.4222	3.5649	3.6071	3.6132	1.4648	1.7111	1.7824	1.8035	1.8066
Charles Chinwuba Ike [54]										1.8065
Sayyad et Ghugal [75]	2.9603	3.4242	3.5654	3.6072	3.6132	1.4802	1.7121	1.7827	1.8038	1.8065

Table 3 provides a highly visual comparison between the theories and methods used by other researchers, which validates our computational model.

This work is not only focused on mechanical buckling, but also includes a program to determine the variation in the critical buckling temperature. Indeed, in the literature, there are only three references related to thermal buckling of concrete: the first is by X. Cheng [65], followed by BENFRID and BACHIR BOUIADJRA MED [64], and also BENFRID and BACHIR BOUIADJRA MED [49]. We used the same values as those mentioned in these three references and executed our program (thermal expansion 10⁻⁵°C, Poisson's ratio 1/3, Young's modulus of concrete 25 GPa). The comparison is presented in Table 4. It is noted that the refined method presented gives results that are closer, but more accurate. This is observed in Table 4, by comparing the programming with recent computational programs.

Table 4A comparison of the thermal buckling ΔT_{cr} of a square isotropic steel plate with variations in the thickness and width parameters.

References	X. Cheng (SD)[65]	BENFRID and BACHIR BOUIADJRA MED (SD)[49]	BENFRID and BACHIR BOUIADJRA MED (FSDT) [64]	Present (The refined FSDT)
b=a; a=30h	146.6	156.6603	156.53	160.6381
b=3a;a=30h	87.1	87.6441	88.21	89.2433
b=a;a=40h	88.1	88.1214	89.31	90.3589
b=3a;a=30h	48.9	48.9563	49.66	50.1994

It is observed in Figure 2 that the critical buckling load in a panel reinforced with glass powder is greater than in a plain concrete panel for a=5h, with a significant margin

at the beginning, when the plate is thin and the b/a ratio is very small. This critical buckling load increases as the b/a ratio increases, and the load becomes nearly equal starting from the b/a=2.5 ratio. It is noted that every time the volume fraction of glass powder increases, the buckling load becomes higher, which means that concrete reinforced with glass powder is more resistant than plain concrete. In Figure 3, it is shown that the critical load for the panel reinforced with glass powder with (a=10h) is higher than that of the panel reinforced with glass powder with (a=5h), as discussed in the previous paragraph. Moreover, it is noted that the critical buckling load for 30% glass powder is always the highest. Similarly, this load starts to decrease as the geometric ratio of width/length increases, until it almost reaches the value of 2.5, where the loads become nearly the same and coincide. It is preferable to state that brick powder also improves the panels more than the first reinforcement, which is glass powder. In Figure 4, the results for a high percentage of glass powder reinforcement in a concrete panel are presented, with the variation in the geometric ratio of length/width, compared with different height/length geometric ratios. It is observed that thinner plates start with a lower buckling load than the others, and as the plate becomes thicker, the load increases. This is logical because the resistance of the beam core section becomes more significant, especially since after a certain thickness, the critical buckling load no longer increases. Furthermore, the reduction in this load varies with the geometric ratio b/a, as already mentioned in the previous paragraphs. Figures 2 to 4 note that the loading is unidirectional.

Figure 2

The mechanical buckling load Unidirectional $N_{cr} = \frac{12(1-v_m^2)a^2N}{E_ch^3}$ of a panel in concrete reinforced with glass powder, with a variation of (b/a) and (a=5h).

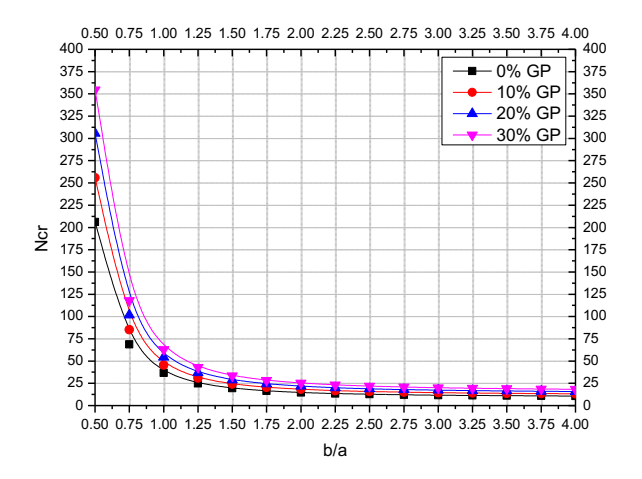
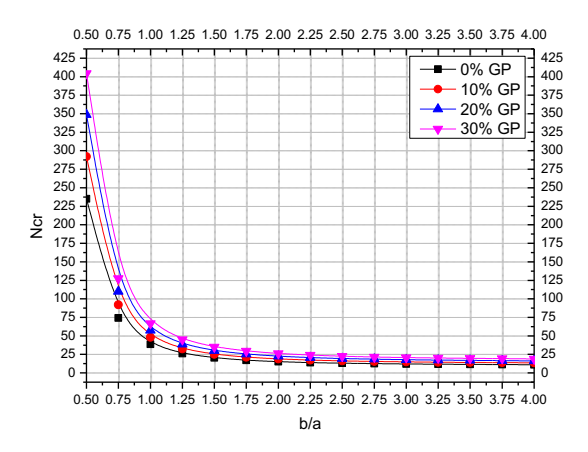


Figure 3

The mechanical buckling load Unidirectional $N_{cr} = \frac{12(1-v_m^2)a^2N}{E_ch^3}$ of a panel in concrete reinforced with glass powder, with a variation of (b/a) and (a=10h).



The mechanical buckling load Unidirectional $N_{cr} = \frac{12(1-v_m^2)a^2N}{E_ch^3}$ of a panel in concrete reinforced with glass powder, with a variation of (b/a) and (a/h) where V_f =30%Gp.

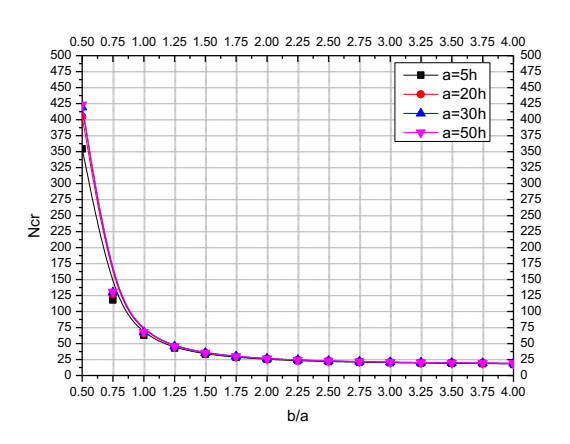


Figure 5

The mechanical buckling load Unidirectional $N_{cr} = \frac{12(1-v_m^2)a^2N}{E_ch^3}$ of a panel in concrete reinforced with brick powder, with a variation of (b/a) and (a=5h).

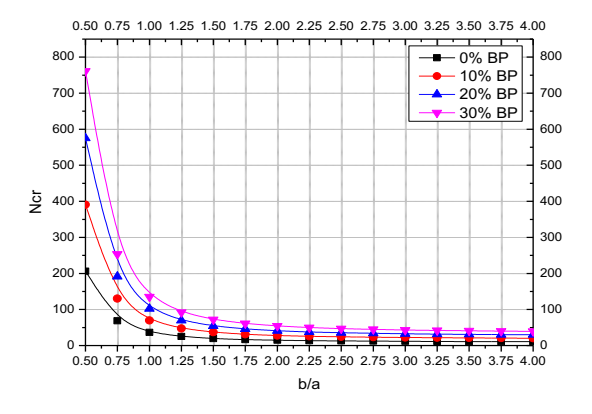


Figure 6

The mechanical buckling load Unidirectional $N_{cr} = \frac{12(1-v_m^2)a^2N}{E_ch^3}$ of a panel in concrete reinforced with brick powder, with a variation of (b/a) and (a=10h).

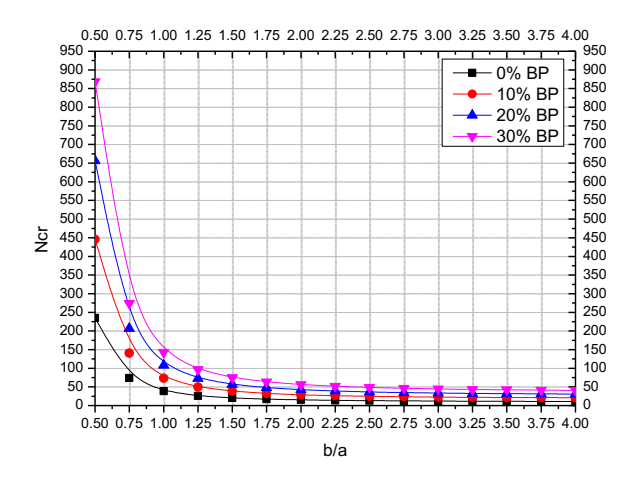


Figure 7

The mechanical buckling load Unidirectional $N_{cr} = \frac{12(1-v_m^2)a^2N}{E_ch^3}$ of a panel in concrete reinforced with glass powder, with a variation of (b/a) and (a/h) where $V_f = 30\%Bp$.

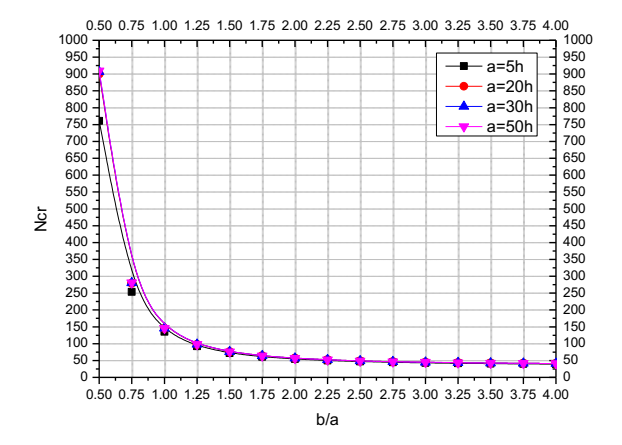


Figure 5 shows that when the plate is thin, with a height/width ratio equal to 5, the critical buckling load is highest for the 30% brick powder fraction. For 10% and 20% brick powder, the efforts are arranged according to the degree of saturation of the brick powder. The lowest critical buckling load is that of plain concrete. The efforts begin to

reduce as the geometric ratio of width/length increases, and they stabilize a bit at the value of 3. Compared with Figure 2, it is clear that glass powder provides higher resistance than brick powder. By reading the values from Figure 6, for (a=10h), all efforts initially increase due to the resistance gained from the inertia of the panel. The same observations are made in the previous figure (Figure 6), but this time, the stabilization of the efforts starts at the (b/a=2) ratio. However, as the geometric ratio of length/width increases, the critical load decreases. Furthermore, in Figure 7, the discussion focuses only on the high fraction of brick powder (30%). The minimum value is observed for low thicknesses, as the inertia is low. This is the same observation as in the discussion of Figure 4. For a panel with (a=50h), it is observed in Table 5 that as the geometric ratio (b/a) increases, the buckling loads decrease. The best results are noted in reinforced concretes, and bricks are more resistant than glass. It is also noted that the volumetric fractions, across the different fractions, improve the critical buckling load. These observations pertain to unidirectional loading.

Table 5 Comparison of the mechanical buckling load Unidirectional $N_{cr} = \frac{12(1-v_m^2)a^2N}{E_ch^3}$ for the different composites and different geometrical parameters and volume fractions when (b/a is variable and a=50h).

	Ordinary	Concre	Concrete with Powder glass			Concrete with Brick powder			
b/a	Concrete.	reinforcement.			reinforcement.				
b/u	Volume	V _f =10%	V _f =20%	V _f =30%	V _f =10%	V _f =20%	V _f =30%		
	fractions								
0.5	246.2540	305.7656	365.2387	423.5278	466.7285	687.5714	909.5381		
0.75	76.0709	94.4548	112.8268	130.8330	144.1783	212.3994	280.9676		
1	39.4473	48.9804	58.5074	67.8446	74.7649	110.1416	145.6983		
1.25	26.5281	32.9391	39.3459	45.6252	50.2791	74.0697	97.9815		
1.5	20.5804	25.5540	30.5244	35.3959	39.0063	57.4630	76.0136		
1.75	17.3583	21.5532	25.7454	29.8542	32.8994	48.4665	64.1128		
2	15.4137	19.1386	22.8612	26.5097	29.2137	43.0368	56.9302		
2.25	14.1471	17.5660	20.9827	24.3314	26.8132	39.5005	52.2523		
2.5	13.2745	16.4825	19.6884	22.8305	25.1593	37.0639	49.0292		
2.75	12.6467	15.7030	18.7573	21.7508	23.9694	35.3110	46.7104		
3	12.1794	15.1227	18.0642	20.9470	23.0837	34.0063	44.9844		
3.25	11.8218	14.6787	17.5338	20.3320	22.4059	33.0078	43.6636		
3.5	11.5418	14.3311	17.1186	19.8505	21.8753	32.2261	42.6296		
3.75	11.3184	14.0537	16.7872	19.4663	21.4519	31.6024	41.8045		
4	11.1372	13.8287	16.5184	19.1546	21.1085	31.0964	41.1351		

The mechanical buckling load Bidirectional $N_{cr} = \frac{12(1-v_m^2)a^2N}{E_ch^3}$ of a panel in concrete reinforced with glass powder, with a variation of (b/a) and (a=5h).

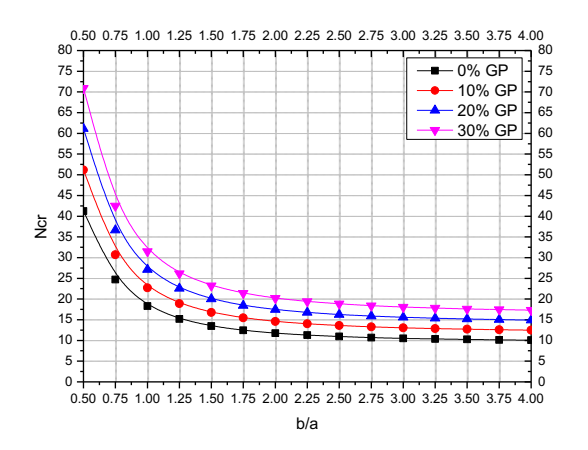
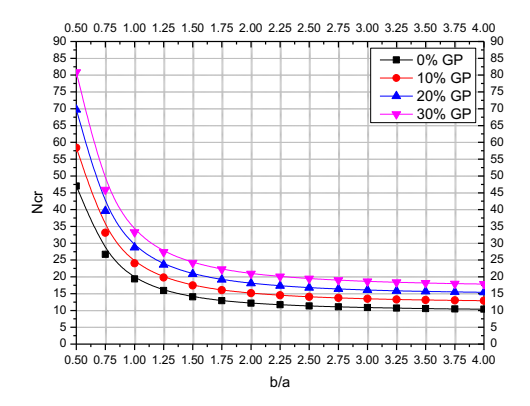


Figure 9

The mechanical buckling load Bidirectional $N_{cr} = \frac{12(1-v_m^2)a^2N}{E_ch^3}$ of a panel in concrete reinforced with glass powder, with a variation of (b/a) and (a=10h).



The mechanical buckling load Bidirectional $N_{cr} = \frac{12(1-v_m^2)a^2N}{E_ch^3}$ of a panel in concrete reinforced with glass powder, with a variation of (b/a) and (a/h) where V_f =30%Gp.

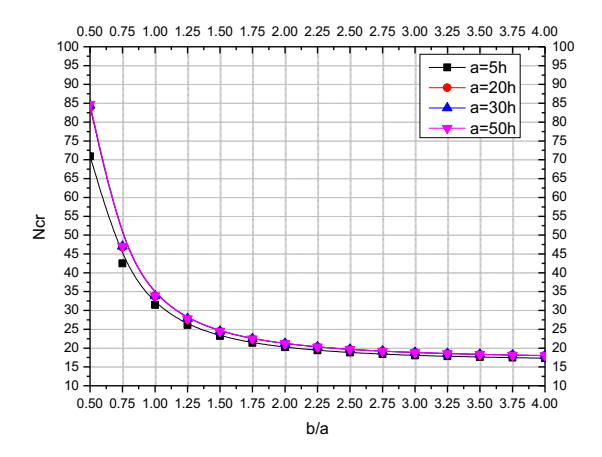
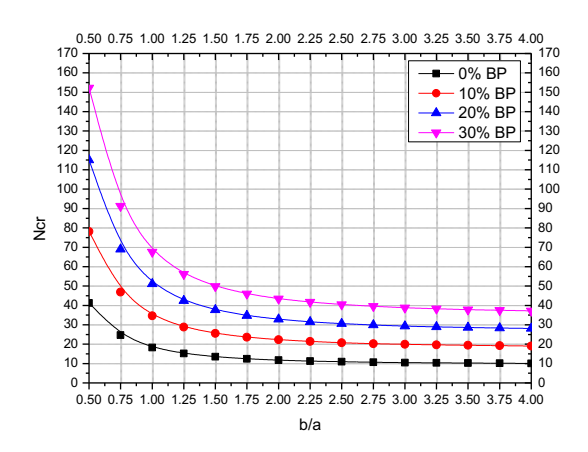


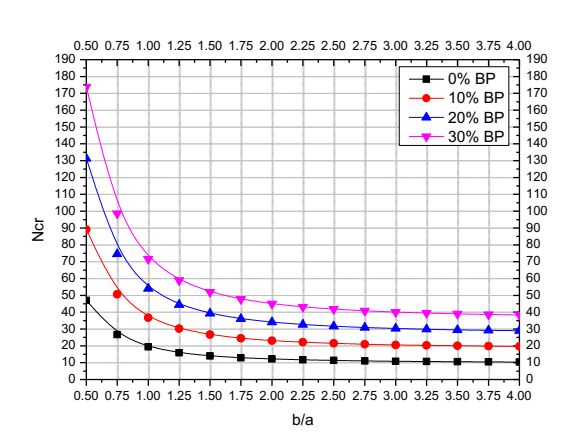
Figure 11

The mechanical buckling load Bidirectional $N_{cr} = \frac{12(1-v_m^2)a^2N}{E_sh^3}$ of a panel in concrete reinforced with brick powder, with a variation of (b/a) and (a=5h).



The mechanical buckling load Bidirectional $N_{cr} = \frac{12(1-v_m^2)a^2N}{E_ch^3}$ of a panel in concrete

reinforced with brick powder, with a variation of (b/a) and (a=10h).



The mechanical buckling load Bidirectional $N_{cr} = \frac{12(1-v_m^2)a^2N}{E_ch^3}$ of a panel in concrete

reinforced with glass powder, with a variation of (b/a) and (a/h) where V_f =30%Bp. For figures 8 to 13, the results are provided in the case of bidirectional loading. Starting with Figure 8 for (a=5h), it is observed that the critical load decreases as the width/length geometric ratio increases. The best results are presented when the volumetric fraction is 30% glass powder. The same observations are made for (a=10h), but with an increase in the critical buckling load value, caused by the resistance of the section, as illustrated in Figure 9. Notably, the best results for 30% show that the critical buckling load is the lowest for the smallest thicknesses. This same observation is made in Figure 13, which represents brick powder. Regarding this reinforcement, it is more resistant than glass, as shown in Figures 11 and 12. Table 6 reflects the same discussions as before, but with well-observed numerical values for a panel of (a=50h).

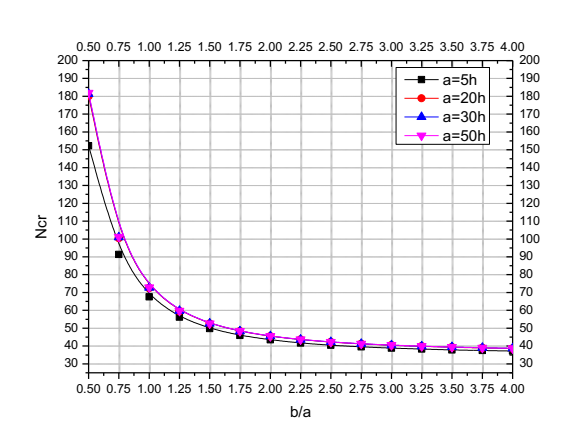


Table 6 $\begin{tabular}{l} \textbf{Comparison of the mechanical buckling load Bidirectional N_{cr}} = \frac{12(1-v_m^2)a^2N}{E_ch^3} for the \\ \begin{tabular}{l} \textbf{different composites and different geometrical parameters and volume fractions when} \\ \textbf{(b/a is variable and a=50h)}. \end{tabular}$

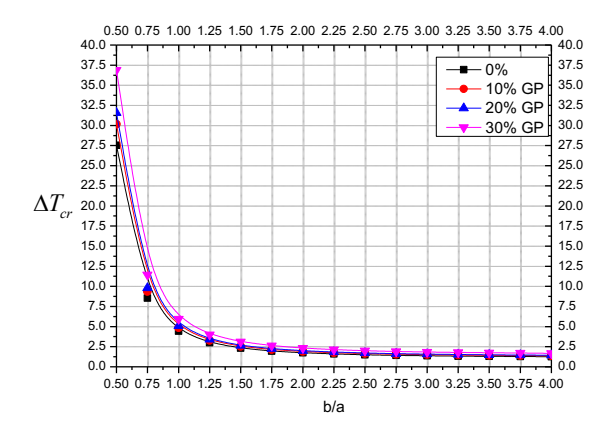
	Ordinary	Concrete with Powder glass			Concrete with Brick powder			
b/a	Concrete.	reinforcement.			reinforcement.			
0/a	Volume	V _f =10%	V _f =20%	V _f =30%	V _f =10%	V _f =20%	V _f =30%	
	fractions							
0.5	49.2508	61.1531	73.0477	84.7056	93.3457	137.5023	181.9672	
0.75	27.3855	34.0037	40.6176	47.0999	51.9042	76.4571	101.1815	
1	19.7236	24.4902	29.2537	33.9223	37.3825	55.0660	72.8730	
1.25	16.1757	20.0848	23.9914	27.8203	30.6580	45.1606	59.7644	
1.5	14.2480	17.6912	21.1323	24.5048	27.0044	39.7786	52.6421	
1.75	13.0855	16.2478	19.4081	22.5055	24.8011	36.5331	48.3470	
2	12.3309	15.3109	18.2890	21.2077	23.3710	34.4265	45.5591	
2.25	11.8136	14.6685	17.5216	20.3179	22.3904	32.9821	43.6477	
2.5	11.4435	14.2090	16.9728	19.6815	21.6890	31.9489	42.2804	
2.75	11.1697	13.8690	16.5666	19.2105	21.1701	31.1844	41.2687	
3	10.9614	13.6104	16.2577	18.8523	20.7753	30.6030	40.4992	
3.25	10.7993	13.4092	16.0173	18.5736	20.4681	30.1505	39.9004	
3.5	10.6707	13.2495	15.8266	18.3524	20.2244	29.7914	39.4252	
3.75	10.5670	13.1207	15.6727	18.1739	20.0277	29.5017	39.0419	
4	10.4821	13.0152	15.5468	18.0279	19.8668	29.2646	38.7281	

Table 7 shows a comparison between glass powder and brick powder with plain concrete. The best results are observed in concrete reinforced with glass powder, where the buckling load decreases as the geometric ratio (b/a) increases. The variation in critical buckling temperature, illustrated in Figure 14, shows that glass powder provides better resistance to thermal buckling than plain concrete. However, the best results are obtained with brick powder, as shown in Figure 15. To confirm that brick powder is the best, two comparisons are made in Figures 16 and 17. It is clearly observed that for volumetric fractions of 30% and 10% of both reinforcements, brick powder provides better results.

Table 7 Comparison of the Variation of the critical buckling temperature ΔT_{cr} for the different composites and different geometrical parameters and volume fractions when (b/a is variable and a=10h).

	Ordinary		te with Powde	_	Concrete with Brick powder				
b/a	Concrete.	ı	reinforcement.			reinforcement.			
D/ a	Volume	V _f =10%	V _f =20%	V _f =30%	V _f =10%	V _f =20%	V _f =30%		
	fractions								
0.5	425.0376	465.4160	487.2565	569.4423	528.8105	563.2400	597.0208		
0.75	133.9849	146.7134	153.5982	179.5056	166.6973	177.5505	188.1992		
1	69.9806	76.6288	80.2247	93.7562	87.0664	92.7350	98.2969		
1.25	47.2195	51.7053	54.1317	63.2621	58.7481	62.5731	66.3259		
1.5	36.6996	40.1860	42.0718	49.1681	45.6598	48.6326	51.5493		
1.75	30.9879	33.9318	35.5241	41.5159	38.5536	41.0637	43.5266		
2	27.5361	30.1520	31.5669	36.8913	34.2590	36.4895	38.6780		
2.25	25.2858	27.6880	28.9873	33.8766	31.4594	33.5076	35.5173		
2.5	23.7344	25.9892	27.2088	31.7981	29.5292	31.4518	33.3381		
2.75	22.6178	24.7665	25.9287	30.3022	28.1400	29.9721	31.7697		
3	21.7864	23.8561	24.9756	29.1882	27.1055	28.8703	30.6018		
3.25	21.1500	23.1592	24.2460	28.3356	26.3137	28.0270	29.7079		
3.5	20.6517	22.6136	23.6747	27.6680	25.6938	27.3666	29.0079		
3.75	20.2539	22.1780	23.2188	27.1351	25.1989	26.8395	28.4493		
4	19.9312	21.8247	22.8489	26.7028	24.7974	26.4119	27.9960		

Figure 14 the Variation of the critical buckling temperature ΔT_{cr} of a panel in concrete reinforced with brick powder, with a variation of (b/a) and (a=20h).



the Variation of the critical buckling temperature ΔT_{cr} of a panel in concrete reinforced with brick powder, with a variation of (b/a) and (a=20h).

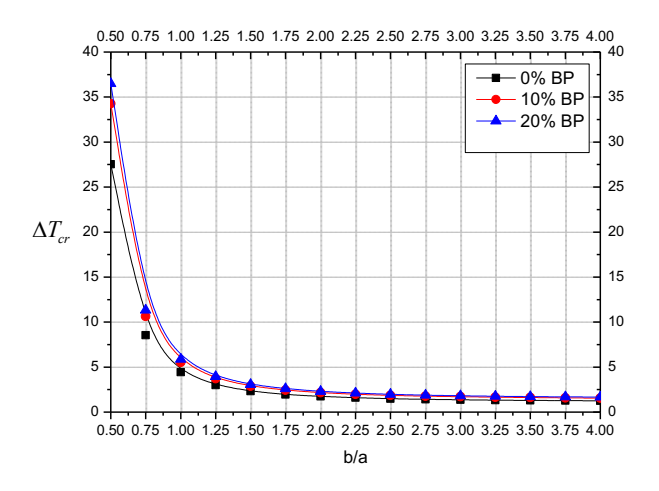


Figure 16

the Variation of the critical buckling temperature ΔT_{cr} of a panel in concrete reinforced with brick powder, with a variation of (b/a) and (a=10h), for (10% Gp or Bp).

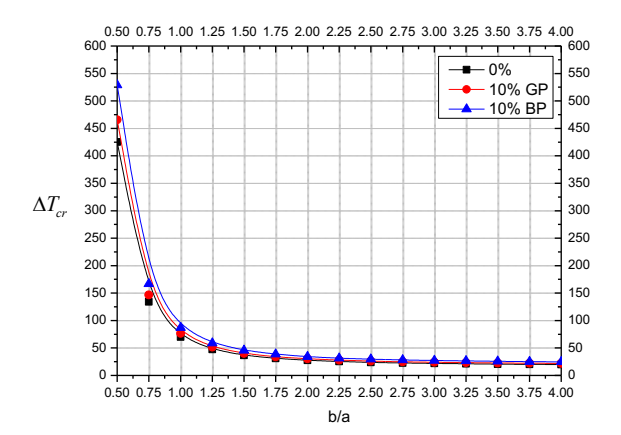
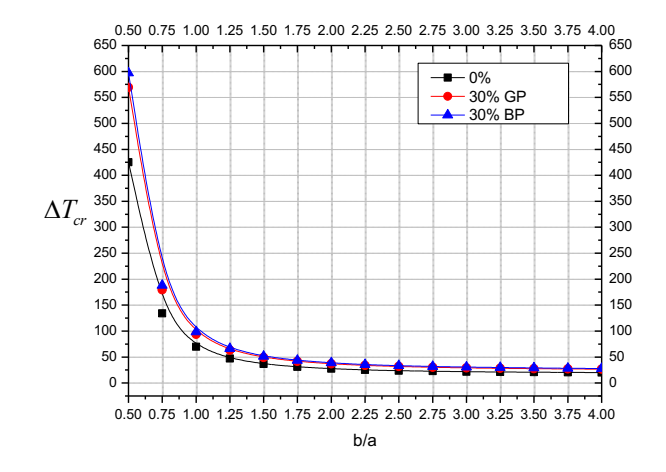


Figure 17 the Variation of the critical buckling temperature ΔT_{cr} of a panel in concrete reinforced with brick powder, with a variation of (b/a) and (a=10h), for (30% Gp or Bp).



5 CONCLUSION

At the end of this work, which focuses on the thermal and mechanical buckling of concrete panels reinforced with glass powder or brick powder, the homogenization step was carried out using the Mori-Tanaka method. A calculation program for the critical buckling load and the variation of the critical temperature was also developed. This program was validated using other references that confirm the validity of the calculation. An improvement in the mechanical properties was observed for both reinforcements, with a notable reduction in thermal expansion, which is beneficial. Furthermore, brick powder yields good results in thermal conductivity calculations, as does glass powder. The critical buckling load increases in the case of reinforced concrete, and the best results are obtained with the highest fractions of glass powder and brick powder. However, brick powder is found to be more effective than glass powder. Geometric parameters also influence the results, as thicker panels resist better than thinner ones. It can also be concluded that the FSDT theory remains valid for solving the issues of panels reinforced with composite materials. Regarding the variation in the critical temperature, the best fraction is 30% for both brick and glass powder, but it is important to note that brick powder is more resistant to thermal buckling than glass powder.

The perspectives of this research:

• Creation of new materials and new durable and resistant concrete.

- Opening of research on the behavior of structures using efficient materials before conducting experiments.
- Revision of national and international calculation standards and regulations.
- Valorization of brick or glass waste for a better environment and improved living conditions.
- Creation of an ecological and economical concrete that could help manage a large range of waste in the construction sector.

REFERENCES

- [1] N. Guermoud, F. Ouadjnia, F. Abdelmalek, F. Taleb, and A. Addou, "Municipal solid waste in Mostaganem city (Western Algeria)," Waste Management, vol. 29, no. 2, pp. 896-902, Feb. 2009, doi: 10.1016/j.wasman.2008.03.027.
- [2] S. Akrour, J. Moore, and S. Grimes, "Évaluation de l'empreinte écologique liée aux activités de consommation et de gestion des déchets des villes du sud de la Méditerranée : cas d'Alger et de Tipaza," Indicateurs Environnementaux et de Durabilité, vol. 12, Dec. 2021, Art. no. 100154, doi: 10.1016/j.indic.2021.100154.
- [3] S. A. Delbari and L. A. Hof, "Glass waste circular economy Advancing to high-value glass sheets recovery using industry 4.0 and 5.0 technologies," Journal of Cleaner Production, vol. 462, Jul. 2024, Art. no. 142629, doi: 10.1016/j.jclepro.2024.142629.
- [4] C. Fu, J. Liang, G. Yang, A. Dagestani, W. Liu, X. Luo, B. Zeng, H. Wu, M. Huang, L. Lin, and X. Deng, "Recycling of waste glass as raw materials for the preparation of self-cleaning, light-weight and high-strength porous ceramics," Journal of Cleaner Production, vol. 317, Oct. 2021, Art. no. 128395, doi: 10.1016/j.jclepro.2021.128395.
- [5] B. Qin, Z. Yao, K. Deng, J. Ruan, and Z. Xu, "Analysis of contaminants and their formation mechanism in the desiccation-dissociation process of organic impurity of waste glass," Journal of Hazardous Materials, vol. 416, Aug. 2021, Art. no. 125881, doi: 10.1016/j.jhazmat.2021.125881.
- [6] M. R. Maaze and S. Shrivastava, "Development and performance evaluation of recycled brick waste-based geopolymer brick for improved physico-mechanical, brick-bond and durability properties," Journal of Building Engineering, vol. 97, Nov. 2024, Art. no. 110701, doi: 10.1016/j.jobe.2024.110701.
- [7] S. El Euch Khay, "Valorisation des matériaux marginaux dans la construction et la réhabilitation des infrastructures," Université de Tunis El Manar, Rapport scientifique, Jun. 2019. [Frensh] (S. El Euch Khay, "Valorization of marginal materials in the construction and rehabilitation of infrastructures," University of Tunis El Manar, Scientific Report, Jun. 2019.)

- [8] I. S. A. Santana, M. da P. Novaes, R. C. C. de Araújo, and L. Batalha-Vieira, "Exposed clay bricks made with waste: An analysis of research and technological trends," Sustainability, vol. 16, no. 24, Art. no. 11274, Dec. 2024, doi: 10.3390/su162411274.
- [9] M. S. Amjad and N. Diaz-Elsayed, "Evaluating the environmental impacts of brick production from waste plastic," Manufacturing Letters, vol. 41, Supplement, pp. 1683-1695, Oct. 2024, doi: 10.1016/j.mfglet.2024.09.196.
- [10] E. Kravchenko, G. Lazorenko, S. Besklubova, and M. H. Raza, "Optimizing carbon dioxide sequestration in waste concrete powder through polymer treatment," Journal of Environmental Chemical Engineering, vol. 13, no. 4, Art. no. 117144, Aug. 2025, doi: 10.1016/j.jece.2025.117144.
- [11] D. A. Muhedin and R. K. Ibrahim, "Effect of waste glass powder as partial replacement of cement & sand in concrete," Case Studies in Construction Materials, vol. 19, Art. no. e02512, Dec. 2023, doi: 10.1016/j.cscm. 2023.e02512.
- [12] B. P. Nugraha, E. T. Sudjatmiko, and I. Bali, "Compressive strength of concrete containing recycled glass powder," PRESUNIVE Civil Engineering Journal, vol. 1, no. 1, pp. 8-12, Apr. 2023.
- [13] K. Khan, W. Ahmad, M. N. Amin, M. I. Rafiq, A. M. Abu Arab, I. A. Alabdullah, H. Alabduljabbar, and A. Mohamed, "Evaluating the effectiveness of waste glass powder for the compressive strength improvement of cement mortar using experimental and machine learning methods," Heliyon, vol. 9, no. 5, Art. no. e16288, May 2023, doi: 10.1016/j.heliyon. 2023.e16288.
- [14] Ö. Zeybek, Y. O. Özkılıç, M. Karalar, A. İ. Çelik, S. Qaidi, J. Ahmad, D. D. Burduhos-Nergis, and D. P. Burduhos-Nergis, "Influence of replacing cement with waste glass on mechanical properties of concrete," Materials (Basel), vol. 15, no. 21, Art. no. 7513, Oct. 2022, doi: 10.3390/ma15217513.
- [15] Y. Diao, L. Chen, and Y. Huang, "Experimental study on mechanical properties of concrete containing waste glass and its application on concrete-filled steel tubular columns," Processes, vol. 11, no. 4, Art. no. 975, Apr. 2023, 10.3390/pr11040975.
- [16] M. M. Salman and M. Z. Yousif, "Mechanical properties of sustainable concrete containing red clay brick waste," International Journal of Modern Engineering Research (IJMER), vol. 8, no. 6, pp. 39, Jun. 2018.
- [17] H. S. Abbas, S. S. Ali, and A. Hassoon, "Using recycled bricks to improve the compressive strength of concrete and produce lightweight concrete," Heritage and Sustainable Development, vol. 5, no. 2, 2023, doi: 10.37868/hsd.v5i2.238.
- [18] S. S. Mansoor, S. M. Hama, and D. N. Hamdullah, "Effectiveness of replacing cement partially with waste brick powder in mortar," Journal of King Saud University - Engineering Sciences, vol. 36, no. 7, pp. 524-532, Nov. 2024, doi: 10.1016/j.jksues.2022.01.004.

- [19] M. S. Nasr, A. J. Salman, R. J. Ghayyib, A. Shubbar, S. Al-Mamoori, Z. Al-khafaji, T. M. Hashim, Z. A. Hasan, and M. Sadique, "Effect of clay brick waste powder on the fresh and hardened properties of self-compacting concrete: State-of-the-art and life cycle assessment," Energies, vol. 16, no. 12, Art. no. 4587, Jun. 2023, doi: 10.3390/en16124587.
- [20] M. S. Nasr, A. J. Salman, R. J. Ghayyib, A. Shubbar, S. Al-Mamoori, Z. Al-khafaji, T. M. Hashim, Z. A. Hasan, and M. Sadique, "Effect of clay brick waste powder on the fresh and hardened properties of self-compacting concrete: State-of-the-art and life cycle assessment," Energies, vol. 16, no. 12, Art. no. 4587, Jun. 2023, doi: 10.3390/en16124587.
- [21] A. Benfrid, A. Benbakhti, Z. R. Harrat, M. Chatbi, B. Krour, and M. B. Bouiadjra, "Thermomechanical analysis of glass powder based eco-concrete panels: Limitations and performance evaluation," Periodica Polytechnica Civil Engineering, vol. 67, no. 4, pp. 1284–1297, 2023, doi: 10.3311/PPci.22781.
- [22] Z. R. Harrat, S. Amziane, B. Krour, and M. B. Bouiadjra, "On the static behavior of nano SiO2 based concrete beams resting on an elastic foundation," Computers and Concrete, vol. 27, no. 6, pp. 575-583, Jun. 2021, doi: 10.12989/cac.2021.27.6.575.
- [23] M. Chatbi, B. Krour, M. A. Benatta, Z. R. Harrat, S. Amziane, and M. B. Bouiadjra, "Bending analysis of nano-SiO2 reinforced concrete slabs resting on elastic foundation," Structural Engineering and Mechanics, vol. 84, no. 5, pp. 685-697, Dec. 2022, doi: 10.12989/sem.2022.84.5.685.
- [24] S. D. Elhennani, Z. R. Harrat, M. Chatbi, A. Belbachir, B. Krour, E. Işık, E. Harirchian, M. Bouremana, and M. B. Bouiadjra, "Buckling and free vibration analyses of various nanoparticle reinforced concrete beams resting on multiparameter elastic foundations," Materials, vol. 16, no. 17, p. 5865, Aug. 2023, doi: 10.3390/ma16175865.
- [25] E. Işık, F. Avcil, M. Hadzima-Nyarko, R. İzol, A. Büyüksaraç, E. Arkan, D. Radu, and Z. Özcan, "Seismic performance and failure mechanisms of reinforced concrete structures subject to the earthquakes in Türkiye," Sustainability, vol. 16, no. 15, p. 6473, Jul. 2024, doi: 10.3390/su16156473.
- [26] E. Işık, D. Radu, E. Harirchian, F. Avcil, E. Arkan, A. Büyüksaraç, and M. Hadzima-Nyarko, "Failures in reinforced-concrete columns and proposals for reinforcement solutions: Insights from the 2023 Kahramanmaraş earthquakes," Buildings, vol. 15, no. 9, p. 1535, May 2025, doi: 10.3390/buildings15091535.
- [27] Z. R. Harrat, M. Chatbi, B. Krour, M. Hadzima-Nyarko, D. Radu, S. Amziane, and M. B. Bouiadjra, "Modeling the thermoelastic bending of ferric oxide (Fe2O3) nanoparticles-enhanced RC slabs," Materials, vol. 16, no. 8, p. 3043, Apr. 2023, doi: 10.3390/ma16083043.
- [28] A. Kecir, M. Chatbi, Z. R. Harrat, M. B. Bouiadjra, M. Bouremana, and B. Krour, "Enhancing the mechanical performance of concrete slabs through the incorporation of nano-sized iron oxide particles (Fe2O3): Non-local bending analysis," Periodica

- Polytechnica Civil Engineering, vol. 68, no. 3, pp. 842-858, 2024, doi: 10.3311/PPci.23016.
- [29] M. Chatbi, Z. R. Harrat, M. A. Benatta, B. Krour, M. Hadzima-Nyarko, E. Işık, S. Czarnecki, and M. B. Bouiadjra, "Nano-clay platelet integration for enhanced bending performance of concrete beams resting on elastic foundation: An analytical investigation," Materials, vol. 16, no. 14, p. 5040, Jul. 2023, 10.3390/ma16145040.
- [30] E. Işık, F. Avcil, R. İzol, A. Büyüksaraç, H. Bilgin, E. Harirchian, and E. Arkan, "Field reconnaissance and earthquake vulnerability of the RC buildings in Adıyaman during 2023 Türkiye earthquakes," Appl. Sci., vol. 14, no. 7, p. 2860, Mar. 2024, doi: 10.3390/app14072860.
- [31] M. Chatbi, Z. R. Harrat, T. Ghazoul, and M. B. Bouiadjra, "Free vibrational analysis of composite beams reinforced with randomly aligned and oriented carbon nanotubes, resting on an elastic foundation," J. Build. Mater. Struct., vol. 9, no. 1, p. 1895, 2022, doi: 10.34118/jbms.v9i1.1895.
- [32] A. Benfrid, M. B. Bouiadjra, A. Benbakhti, S. D. El Hannani, B. Krour, M. Chatbi, and Z. R. Harrat, "Attaining energy conservation in buildings through the integration of barley organic fibers into construction concrete for thermal insulation," in Modeling, Analysis, and Control of Smart Energy Systems, 2024, pp. 26, doi: 10.4018/979-8-3693-2999-3.ch009.
- [33] A. Benbakhti, A. Benfrid, Z. R. Harrat, M. Chatbi, M. B. Bouiadjra, and B. Krour, "An analytical analysis of the hydrostatic bending to design a wastewater treatment plant by a new advanced composite material," RCMA, vol. 34, no. 2, pp. 177-188, 2024, doi: 10.18280/rcma.340207.
- [34] J. Zhou, H. Lin, K. Qiu, K. Ou, and F. Nie, "Prediction of modulus of elasticity of concrete using different homogenization methods," Materials, vol. 18, no. 12, p. 2674, 2025, doi: 10.3390/ma18122674.
- [35] S. Lu, Z. Zhang, Y. Du, and D. Zhao, "Research on the structural traits and upscaling of parameters of ITZ within multi-scale carbon-based fiber strengthened concrete". https://doi.org/10.21203/rs.3.rs-7055929/v1.
- [36] Q. Chen, H. Zhu, Z. Yan, T. Deng, and S. Zhou, "Microscopic description of electrochemical deposition repair of saturated concrete based on the Mori-Tanaka method," Journal of Civil Engineering and Architecture, vol. 2015, no. 1, 2015, Art. no. 10.14006/j.jzjgxb.2015.01.013.
- [37] A. Benfrid, M. Bouiadjra, M. Chatbi, and Z. Harrat, "Impact of glass nanoparticles on the elastic modulus of concrete," University of Zawia Journal of Engineering Sciences and Technology, Civil Engineering, vol. 2, no. 2, p. 16, Dec. 2024, doi: 10.26629/uzjest.2024.16.

- [38] Wang, Y., & Liu, J. (2024). Theoretical investigation on elastic property evolutions of low volume fly ash concrete. Journal of the American Ceramic Society. https://doi.org/10.1111/jace.20127.
- [39] S. Yan, B. Wang, Y. Sun, and B. Lyu, "Micromechanics-based prediction models and experimental validation on elastic modulus of recycled aggregate concrete," Sustainability, vol. 13, no. 20, p. 11172, Oct. 2021, doi: 10.3390/su132011172.
- [40] T. Mori and K. Tanaka, "Average stress in matrix and average elastic energy of materials with misfitting inclusions," Acta Metallurgica, vol. 21, no. 5, pp. 571-574, May 1973, doi: 10.1016/0001-6160(73)90064-3.
- [41] K. Murawski, A. Shvets, and L. P. Kiss, "FEM buckling, stress, and strain analysis of very slender rectangular (box-section) columns fixed at one end," Stability of Structures Journal of Critical Engineering, 2025. https://www.lulu.com/account/projects/7k99wrj.
- [42] A. Doicheva, "T-shaped frame critical and post-critical analysis," Journal of Theoretical and Applied Mechanics (Bulgaria), vol. 46, no. 1, pp. 65-82, 2016. doi: 10.1515/jtam-2016-0005.
- [43] A. Doicheva, "Exact solution for a beam on off-center spring supports," Journal of Theoretical and Applied Mechanics (Bulgaria), vol. 41, no. 2, pp. 69-82, 2011.
- [44] K. Mladenov and A. Doicheva, "Critical and post-critical analysis of water tower with conical tank," Annual of the University of Architecture, Civil Engineering and Geodezy UACEG, vol. 49, no. 2, pp. 63-76, 2016. Available: https://annual.uacg.bg/article/2016_49_2_07.
- [45] K. Mladenov and A. Doicheva, "On some illustrative potentialities of simply supported beams," in 11th National Congress on Theoretical and Applied Mechanics, Borovets, Bulgaria, 2009. Available: http://nctam.imbm.bas.bg/index.php/nctam/nctam2009/paper/viewFile/127/43.
- [46] K. Mladenov and A. Doicheva, "Bending-torsional buckling of a beam on elastic rotational springs," Civil Engineering Bulgaria, no. 6, pp. 2-7, 2008. ISSN 0562-1852.
- [47] A. Doicheva and K. Mladenov, "An approach to determining critical loading for off-center supported beams," Days of Mechanics Varna, Mechanics of Machines Magazine, vol. XX, Book 1, pp. 38-41, 2012. ISSN 0861-9727.
- [48] K. Mladenov and A. Doicheva, "Flexural-torsional buckling of an off-center supported beam," in Annual of University of Architecture, Civil Engineering and Geodezy Sofia, vol. XLIV, International Conference UACEG2009: Science and Practice, Sofia, Bulgaria, 2009, pp. 103-114. ISSN 1310-814X.
- [49] A. Benfrid and M. B. Bouiadjra, "Investigation of instability in waste glass-based eco-concrete panels under thermomechanical buckling loads," Studies in Engineering and Exact Sciences, vol. 5, no. 2, 2024, doi: 10.54021/seesv5n2-108.

- [50] H. Khetir, A. Benfrid, M. B. Bouiadjra, R. Z. Harrat, and M. Chatbi, "Mechanical instabilities of nano-composite plates using elasticity theories," Studies in Engineering and Exact Sciences, vol. 5, no. 2, Article 009, 2024. doi: 10.54021/seesv5n2-009.
- [51] N. Enoma and J. Madu, "Buckling of Externally Pressurized Toroidal Vessels with Circular-Elliptical Cross-Section," NIPES - Journal of Science and Technology Research, vol. 4, no. 2, 2022. https://doi.org/10.37933/nipes/4.2.2022.26.
- [52] N. Enoma and J. Madu, "Effect of Imperfections on the Buckling Behaviour of a Pressurized Circular-Elliptical Toroid," NIPES - Journal of Science and Technology Research, vol. 4, no. 2, 2022. https://doi.org/10.37933/nipes/4.2.2022.27.
- [53] I. C. Chinwuba, "Buckling Analysis of Relatively Thick Plates using First Order Shear Deformation Plate Theory: Exact Solutions," NIPES - Journal of Science and Research, vol. Technology 7, no. 2, pp. 23–43. 2025. [Online]. https://doi.org/10.37933/nipes/7.2.2025.2.
- [54] I. C., "Variational Formulations of Exponential Shear Deformable Plate Buckling Problems and Analytical Solutions Using Double Fourier Series Method," NIPES -Journal of Science and Technology Research, vol. 7, no. 3, pp. 31-50, 2025. https://doi.org/10.37933/nipes/7.3.2025.3.
- [55] C. C. Ike, "Analysis of Single Variable Thick Plate Buckling Problems using Galerkin Method," NIPES - Journal of Science and Technology Research, vol. 7, no. 2, pp. 235-252, 2025. [Online]. Available: https://doi.org/10.37933/nipes/7.2.2025.16.
- [56] C. Ike and J. N. Ugwu, "First Principles Ritz Variational Formulation for Buckling Analysis of Polynomial Shear Deformable Beams: Analytical Solutions," NIPES -Journal of Science and Technology Research, vol. 7, no. 3, pp. 1–18, 2025. https://doi.org/10.37933/nipes/7.3.2025.
- [57] P. Pramod Kumar, S. Madhu, and V. V. Subba Rao, "Correlation of CLPT and FSDT Responses in CNT/Polymer Composite Beams Under Deflection and Buckling," Int. J. Recent Technol. Eng., vol. 8, no. 2, pp. 5240-5344, Jul. 2019. https://doi.org/10.35940/ijrte.B1053.078219.
- [58] S. Das and P. Jana, "Analytical Solution for Buckling of Rectangular Plate Subjected to Non-uniform Uniaxial Compression Using FSDT," in Recent Advances in Computational and Experimental Mechanics, Vol II, D. K. Maiti et al., Eds. Singapore: Springer, 2022, pp. 637–647. https://doi.org/10.1007/978-981-16-6490-8 40.
- [59] I. Senjanović, N. Vladimir, and M. Tomić, "On new first-order shear deformation plate theories," Mechanics Research Communications, vol. 73, pp. 31–38, Apr. 2016. https://doi.org/10.1016/j.mechrescom.2016.02.005.

- [60] P. J. Guruprasad and K. S. Pakhare, "Single variable new first-order shear deformation theory for isotropic plates," Lat. Am. J. Solids Struct., vol. 15, no. 10, 2018. https://doi.org/10.1590/1679-78254842.
- [61] S. A. M. Ghannadpour, H. R. Ovesy, and E. Zia-Dehkordi, "Buckling and post-buckling behaviour of moderately thick plates using an exact finite strip," Computers & Structures, vol. 147, pp. 172–180, Jan. 2015. https://doi.org/10.1016/j.compstruc.2014.09.013.
- [62] B. Xu, L. Wang, C. Xiang, and Z. Han, "Analysis of Buckling Deformation for the Side Plate of Rectangular CSFT Column Based on Plate Theory with Bi-Axial Loads," Buildings, vol. 12, no. 5, art. 626, May 2022. https://doi.org/10.3390/buildings12050626.
- [63] S. E. Swartz and V. H. Rosebraugh, "Buckling of Reinforced Concrete Plates," Journal of the Structural Division, vol. 100, no. 1, Jan. 1974. https://doi.org/10.1061/JSDEAG.0003691.
- [64] A. Benfrid, M. B. Bouiadjra, M. Chatbi, Z. R. Harrat, et al., "Model physics to calculate the thermal buckling of a thin eco-panel in concretereinforced by cow bones," Middle East J. Sci. Publ., vol. 7, no. 2, 2024.
- [65] X. Cheng, Thermal Elastic Mechanics Problems of Concrete Rectangular Thin Plate. Springer, 2018. 9811044724.
- [66] L. C. Zhao, S. S. Chen, and J. Cheng, "Thermal buckling analysis of concrete rectangular thin plates considering material damage," Arch. Appl. Mech., vol. 92, pp. 3447–3454, 2022. https://doi.org/10.1007/s00419-022-02289-w.
- [67] H. Wang, G. Yan, and Y. Khairy, "Thermal buckling of the concrete structures reinforced by nanocomposites: Introducing advanced deep neural networks for thermal buckling problem," Mechanics of Advanced Materials and Structures, vol. 32, no. 6, pp. 1211–1224, 2025. https://doi.org/10.1080/15376494.2024.2361447.
- [68] A. Sauvageon, G. Hervé-Secourgeon, C. De Sa, P. Wyniecki, and R. Bennacer, "A simplified method for thermal buckling verification in steel—concrete composite elements," Journal of Constructional Steel Research, vol. 214, art. 108433, Mar. 2024. https://doi.org/10.1016/j.jcsr.2023.108433.
- [69] M. Zhou, G. Yan, D. Hu, and H. A. Mahmoud, "Thermal post-buckling measurement of the advanced nanocomposites reinforced concrete systems via both mathematical modeling and machine learning algorithm," Advances in Nano Research, vol. 16, no. 6, pp. 623–638, Jun. 2024. https://doi.org/10.12989/anr.2024.16.6.623.
- [70] A. Sauvageon, R. Bennacer, C. De-Sa, P. Wyniecki, and J. Niepceron, "Numerical Study of Local Buckling for Steel-Concrete Composite Structures Under Thermal Loadings," 2nd Conference on Technological Innovations in Nuclear Civil Engineering (TINCE 2014), Paris, France, Sep. 1-4, 2014.
- [71] G. S. M. Gunjal, R. B. Hajare, A. S. Sayyad, and M. D. Ghodle, "Buckling Analysis Of Thick Plates Using Refined Trigonometric Shear Deformation Theory," Journal

- of Materials and Engineering Structures, vol. 2, no. 4, pp. 159–167, Dec. 30, 2015. https://asjp.cerist.dz/en/article/117930
- [72] B. M. Shinde, A. S. Sayyad, and A. B. Kawade, "Thermal analysis of isotropic plates using hyperbolic shear deformation theory," Applied and Computational Mechanics, vol. 7, pp. 193–204, 2013.
- [73] M. Bouazza and E. A. Adda-Bedia, "Elastic stability of functionally graded rectangular plates under mechanical and thermal loadings," Scientific Research and Essays, vol. 8, no. 39, pp. 1933–1943, Oct. 18, 2013. DOI: 10.5897/SRE11.251.
- [74] A. S. Sayyad and Y. M. Ghugal, "Buckling analysis of thick isotropic plates by using exponential shear deformation theory," Applied and Computational Mechanics, vol. 6, pp. 185–196, 2012.
- [75] A. S. Sayyad, B. M. Shinde, and Y. M. Ghugal, "Bending, vibration and buckling of laminated composite plates using a simple four variable plate theory," Lat. Am. J. Solids Struct., vol. 13, no. 3, Mar. 2016. https://doi.org/10.1590/1679-78252241.
- [76] E. Postek and T. Sadowski, "Impact model of the Al₂O₃/ZrO₂ composite by peridynamics," Composite Structures, vol. 271, p. 114071, Sep. 2021, doi: 10.1016/j.compstruct.2021.114071.

Acknowledgement

The project presented in this article is supported by the laboratory of advanced structures and materials in civil engineering and public works, Sidi Bel-Abbes, Algeria.

This research is included in the axes of the Thematic Agency for Research in Science and Technology (ATRST), 16000 Algiers, Algeria.